# Tunneling in Chains of Quantum Dots

**J. Planelles* and J. L. Movilla**

*Departament de Ciències Experimentals, Universitat Jaume I, 12080 Castelló, Spain*

*Received: May 10, 2004; In Final Form: June 25, 2004*

The definition of time-dependent overlap between Wannier functions is introduced to estimate electron mobility in a periodic lattice. Time evolution studies carried out in simple band models yield an easy analysis of the role of bandwidth and density-of-states on tunneling time. Comparison of tunneling times in one-dimensional superlattices built of both homogeneous semiconductor quantum dots and two-shell semiconductor antidot nanocrystals reveals that while a monotonic increasing in electron mobility vs nanocrystal density can be seen in the first case, a maximum in mobility is found in the second kind of superlattices for a critical value of the nanocrystal density.

## 1. Introduction

Arrays of semiconductor quantum dots with precisely controlled particle size and interparticle distance are expected to be widely applicable to key devices in electronics, including ultra-large-scale integrated circuits, thin-film transistors for liquid crystal displays, solar cells, etc. Interdot interaction is expected to provide new functions in electron transport since, in a sequence of identical nanocrystals, the discrete 0D states develop into minibands.[1,2] Weak coupling yields narrow bands and large gaps, while strong coupling results in wide bands and small gaps. The band gaps between minibands are also largely dependent upon the building block particle design (size, shape, and composition), while bandwidths can be controlled by the tunneling distance (nanocrystal density). The experimental transport characteristics of linear QD array leads clearly reflect the formation of a miniband structure[3,4] and can thus be controlled by the design of the array (tailoring). Electrical conductivity is in fact an electron flux and therefore requires net electron momentum. Because of the symmetry of the band energy dispersion, $E(k) = E(-k)$, for each occupied state $\phi_k$ there would be an occupied partner $\phi_{-k}$. In short, each electron with momentum $\hbar k$ would be balanced by another with momentum $-\hbar k$, and the net momentum and electrical current would be zero. However, if we apply an external electric field, the $\phi_k$ and $\phi_{-k}$ states lose their degeneracy, so that the states corresponding to the motion following the direction of lower potential will have lower energy and the electric current will flow. Electric conductivity is dependent upon the voltage that is applied but it is also a function of the intrinsic mobility of an electron in a given medium, i.e., a function of the tunneling time $\tau$ required by an electron initially located in a given superlattice cell to go into the next one.

Some fundamental aspects of superlattice physics have been recently reviewed.[5] We provide in this paper a quick and easy estimation of the mobility of an electron, initially injected (localized) in a given cell in a quantum dot superlattice. Since Wannier functions are those that are maximally localized,[6,7] we assume that the injected electron is described by a nonstationary Wannier function that evolves with time. Striking electron mobility differences found in homogeneous dot and antidot superlattices are discussed.

## 2. Wannier Functions

Wannier functions are localized linear combinations of Bloch stationary waves $\phi_{n,k}$ of a given band

$$\omega(n,\mathbf{r}) = \left(\frac{b}{2\pi}\right)^{1/2} \int_{-\pi/b}^{\pi/b} \phi_{n,k}(\mathbf{r})\, \mathrm{d}k \qquad (1)$$

In the above equation, $n = 1, 2, 3, \ldots$ labels the band, $k \in [-\pi/b,\pi/b]$ labels the states within a band, and $b$ is the superlattice constant. Since we will be working within one band at a time, we will hereafter omit the band label $n$.

The Bloch waves are defined up to a phase factor, and therefore, eq 1 does not provide a complete definition of $\omega(\mathbf{r})$. We will implicitly assume the Kohn phase factor criterion that ensures a maximal localization in one-dimensional lattices.[6] With this criterion, eq 1 represents a localized state centered on the reference "0" cell. We will then supply the Wannier function with an extra cell-label; i.e., we will write $\omega_0(\mathbf{r})$ in order to specify the Wannier function centering site.

However, we can also center the Wannier function on another cell $G$ by means of a shift

$$\hat{t}_G \omega_0(\mathbf{r}) = \omega_0(\hat{t}_G{}^{-1}\mathbf{r}) = \omega_0(\mathbf{r} - \mathbf{i}Gb) \equiv \omega_G(\mathbf{r}) \qquad (2)$$

where $b$ is the superlattice constant.

Since

$$\hat{t}_G \phi_k(\mathbf{r}) = \phi_k(\hat{t}_G{}^{-1}\mathbf{r}) = \mathrm{e}^{-ikGb}\phi_k(\mathbf{r}) \qquad (3)$$

from eq 1, we have

$$\omega_G(\mathbf{r}) = \omega_0(\hat{t}_G{}^{-1}\mathbf{r}) = \omega_0(\mathbf{r} - \mathbf{i}Gb) = \left(\frac{b}{2\pi}\right)^{1/2} \int_{-\pi/b}^{\pi/b} \mathrm{e}^{-ikGb}\phi_k(\mathbf{r})\, \mathrm{d}k \qquad (4)$$

which relates a Wannier function localized on cell $G$ to the set of Bloch waves $\phi_k(\mathbf{r})$.

* Corresponding author. E-mail: planelle@exp.uji.es.

10.1021/jp048007g CCC: $27.50 
Published on Web 08/07/2004

We should note that the Bloch functions are defined in all the space but are normalized in the unit cell:

$$\int_{-\infty}^{\infty}\int_{-\infty}^{\infty}\int_{x=-b/2}^{x=b/2}\phi_k(\mathbf{r})^*\phi_{k'}(\mathbf{r})\,\mathrm{d}v = \frac{b}{2\pi}\delta_{k,k'} \tag{5}$$

In the full space they are normalized to the Dirac $\delta$:

$$\int_{-\infty}^{\infty}\phi_k^*\phi_{k'}\,\mathrm{d}v = \sum_H\int_{-b/2+Hb}^{b/2+Hb}\phi_k^*\phi_{k'}\,\mathrm{d}v = \delta(k-k') \tag{6}$$

From eqs 1 and 6 we can see that the Wannier functions are normalized to unity in the full space:

$$\int_{-\infty}^{\infty}\omega_G(\mathbf{r})^*\omega_{G'}(\mathbf{r})\,\mathrm{d}r = \delta_{G,G'} \tag{7}$$

### 3. Time-Dependent Wannier Function

A Wannier function, as in eq 4, is not an eigenfunction of the periodic Hamiltonian but a linear combination of eigenvectors whose expectation energy value is the average of the band energy:

$$E_G = \int_{-\infty}^{\infty}\omega_G(\mathbf{r})^*\hat{\mathscr{H}}\omega_{G'}(\mathbf{r})\,\mathrm{d}\mathbf{r} = \frac{b}{2\pi}\int_{-\pi/b}^{\pi/b}\int_{-\pi/b}^{\pi/b}\mathrm{d}k\,\mathrm{d}k'\,\mathrm{e}^{iG(k-k')b}E(k')\int_{-\infty}^{\infty}\mathrm{d}\mathbf{r}\,\phi_k(\mathbf{r})^*\,\phi_{k'}(\mathbf{r}) = \frac{b}{2\pi}\int_{-\pi/b}^{\pi/b}E(k)\,\mathrm{d}k = \frac{1}{2\pi}\int_{-\pi}^{\pi}E(k)\,\mathrm{d}k \tag{8}$$

This nonstationary state evolves with time as follows

$$\omega_G(\mathbf{r},t) = \left(\frac{b}{2\pi}\right)^{1/2}\int_{-\pi/b}^{\pi/b}\mathrm{e}^{-ikGb}\mathrm{e}^{-iE(k)t/\hbar}\phi_k(\mathbf{r})\,\mathrm{d}k \tag{9}$$

so that eq 4 is the particular case in which $t = 0$ in eq 9.

In the empty lattice case, i.e., if the crystal periodic potential is just a constant, the Bloch waves just become $\phi_k(\mathbf{r}) = (1/2\pi)^{1/2}\mathrm{e}^{ik\mathbf{r}}$. Then, by defining

$$c(k) = \begin{cases}\sqrt{b}\mathrm{e}^{-ikGb} & -\dfrac{\pi}{b} \le k \le \dfrac{\pi}{b}\\ 0 & \text{otherwise}\end{cases} \tag{10}$$

we may (formally) identify eq 9 with a wave packet $W(x,t)$.

$$W(x,t) = \int_{-\infty}^{\infty}c(k)\mathrm{e}^{-iE(k)t/\hbar}\mathrm{e}^{ikx}\,\mathrm{d}k \tag{11}$$

However, in a wave packet, $c(k)$ is a Gaussian function, $c(k) = (2\sigma_0{}^2\pi^3)^{-1/4}e^{-(k-k_0)^2/\sigma^2}$, instead of a phase factor as in eq 9. Therefore, one cannot expect the same time evolution behavior for both nonstationary states, but we do expect there to be some similarities.

A wave packet is a Gaussian function with a maximum at $x = \hbar k_0 t/m$ and a growing time-dependent half-width $\sigma(t) = |\sigma_0 + (i\hbar\sigma_0/2m)t|$ that moves at a constant speed $v = \hbar k_0/m$; i.e., the packet moves and, simultaneously, is smeared out with time. However, its momentum expectation value remains constant. We will show later on that a Wannier state, like the wave packet, smears out almost time-linearly and its energy expectation value is also constant. However, the Wannier states do not have a net momentum; i.e., this is equal to zero at any particular time.

### 4. Electron Mobility

In the above section, it is stated that a Wannier state does not move. However, we can use it to estimate the electron mobility in a given superlattice. To this end, let us suppose that we initially inject ($t = 0$) an electron in a given cell $G$ (i.e., we localize the electron in $G$). Equation 4 gives us its initial density distribution and eq 9 provides the corresponding time evolution. We can see how the electron travels along the 1D crystal by plotting the time evolution of $|\omega_G(\mathbf{r},t)|^2$ and we can also estimate the tunneling time $\tau$ required by the electron (which is initially localized in cell $G$) to go to another $G'$ cell as the time required by the time-dependent overlap

$$|\,c(t)|^2 = |\langle\omega_{G'}(\mathbf{r},0)|\omega_G(\mathbf{r},t)\rangle|^2 \tag{12}$$

to reach its first maximum. Indeed, from the orthogonality of Wannier functions, it is obvious that if $G \neq G'$ the overlap at $t = 0$, $c(0)$, is zero. However, as time goes by, $c(t)$ is no longer equal to zero and its value is given by

$$c(t) = \langle\omega_{G'}(\mathbf{r},0)|\omega_G(\mathbf{r},t)\rangle = \frac{b}{2\pi}\int_{-\pi/b}^{\pi/b}\int_{-\pi/b}^{\pi/b}\mathrm{d}k_1\,\mathrm{d}k_2\,\mathrm{e}^{ik_1G'b}\mathrm{e}^{-ik_2Gb}\mathrm{e}^{-iE(k_2)t/\hbar}\times\int_{-\infty}^{\infty}\mathrm{d}\mathbf{r}\,\phi_{k_1}(\mathbf{r})^*\,\phi_{k_2}(\mathbf{r}) = \frac{1}{2\pi}\int_{-\pi}^{\pi}\mathrm{e}^{i[(G-G')k-E(k)t/\hbar]}\,\mathrm{d}k \tag{13}$$

### 5. Time Evolution in Simple Band Models

In this section we consider the two simplest band models, namely the parabolic model

$$E_\mathrm{p}(k) = \alpha\left(\frac{kb}{\pi}\right)^2 \tag{14}$$

where $\alpha$ is the bandwidth and $b$ is the lattice constant, and a second model defined by[14]

$$E_\mathrm{s}(k) = \alpha\sin\left(\frac{kb}{2}\right)^2 \tag{15}$$

The first model corresponds to the empty lattice. The second one is very similar to the first but it supplies the energy dispersion with a zero derivative vs $k$ at the band edge, in an attempt to mimic how the periodic lattice potential opens energy gaps and then produces severe changes in energy curvature in the region of the band edge.

The time-dependent overlap, eq 13, turns into

$$c_\mathrm{p}(t) = \frac{1}{2\pi}\int_{-\pi}^{\pi}\mathrm{e}^{i[(G-G')k-\alpha(k/\pi)^2t/\hbar]}\,\mathrm{d}k \tag{16}$$

and

$$c_\mathrm{s}(t) = \frac{1}{2\pi}\int_{-\pi}^{\pi}\mathrm{e}^{i[(G-G')k-\alpha\sin(k/2)^2t/\hbar]}\,\mathrm{d}k \tag{17}$$

Both models yield similar plots of the time-dependent overlap vs time and similar tunneling times $\tau$. As an example we show in Figure 1 the evolution of the time-dependent overlap $c_\mathrm{p}(t)$ between a Wannier function $\omega_{G'}(\mathbf{r},0)$ and another $\omega_G(\mathbf{r},t)$, with $G - G' = 5$, which corresponds to a parabolic band defined by a bandwidth $\Delta E = 0.1$ au. In Table 1 we also include the time $\tau_5$ required by $|c_\mathrm{p}(t)|^2$ to reach its first maximum for $\Delta G = 5$ and different bandwidths. Almost the same times are also yielded by $|c_\mathrm{s}(t)|^2$. Other models, such as $E(k) = \alpha(kb/\pi)^4$, may yield however quite different $\tau$ times.

This table evidences a reciprocal relationship between the tunneling time $\tau$ and the bandwidth. In addition, the density of states, DOS, exerts an influence on the value of $\tau$, as comes

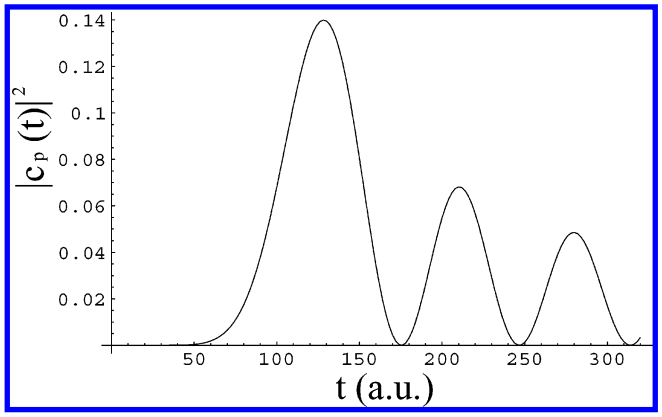


**Figure 1.** Time-dependent overlap $|c_p(t)|^2$, eq 16, vs time between $\omega_{G'}(\mathbf{r},0)$ and $\omega_G(\mathbf{r},t)$, with $G - G' = 5$, for a parabolic band model defined by a bandwidth $\Delta E = 0.1$ au.

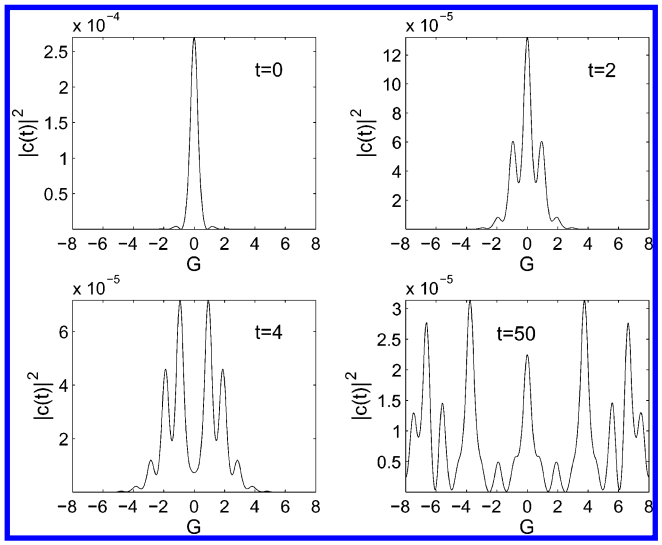


**Figure 2.** Plots of electron density distributions of a time-dependent Wannier state at different times (au).

**TABLE 1: Tunneling Time $\tau_5$ Required by a Parabolic Band Electron To Reach the Fifth Cell, for Different Bandwidths $\Delta E$**

| $\Delta E$ (au) | $\tau_5$ (au) |
|---|---|
| 0.1 | 125.0 |
| 1 | 12.5 |
| 10 | 1.25 |
| 25 | 0.50 |

out from the fact that different energy dispersion models with the same bandwidth may yield different tunneling times.

Finally, we show in Figure 2 how a Wannier function is smeared out with time, and in Figure 3 we have plotted the time required by an electron to reach consecutive cells, i.e., the time $\tau_G$ required by $|c(t)|^2$ to reach its first maximum in the $G$th cell vs $G$, for different band models. This figure reveals that the time-dependent Wannier function smears out almost linearly vs time, like the half-width of a Gaussian packet.

To end this section, we study the influence exerted by periodicity on tunneling time $\tau$. To do so an isolated double-well is considered. If the central barrier is high and wide, we will find an almost two-degenerate ground energy state, which associated eigenvectors, $\Psi_+$ and $\Psi_-$, show even/odd symmetry, respectively. As we reduce the barrier, the even state stabilizes while the odd one becomes more unstable so that an energy splitting $\Delta E = E_- - E_+$ is produced. We may write functions that are maximally localized in a given well at an arbitrary time

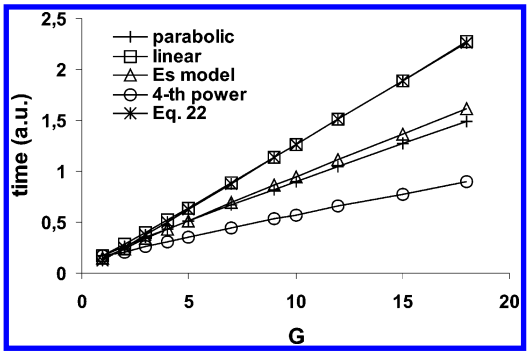


**Figure 3.** Tunneling time $\tau_G$ required by an electron to reach the $G$th cell vs $G$ (defined as the time required by $|c(t)|^2$, eq 13, to attain its first maximum in the $G$th cell) for different band models. $\tau_G$ estimated by eq 22 is also included.

$t = 0$ as linear combinations of the abovementioned eigenvectors:

$$\Psi_L = \frac{1}{\sqrt{2}}(\Psi_+ + \Psi_-) \tag{18}$$

$$\Psi_R = \frac{1}{\sqrt{2}}(\Psi_+ - \Psi_-) \tag{19}$$

However, they do not remain localized with the passage of time. For example, explicitly writing the time in $\Psi_L$ we have

$$\Psi_L = \frac{1}{\sqrt{2}}(\Psi_+ e^{-iE_+t/\hbar} + \Psi_- e^{-iE-t/\hbar}) \tag{20}$$

and therefore

$$|\Psi_L|^2 = \frac{1}{2}\left(|\Psi_+|^2 + |\Psi_-|^2 + 2\Psi_+\Psi_- \cos\frac{\Delta E t}{\hbar}\right) \tag{21}$$

At $t = 0$ this density has a maximum in the well on the left, $|\Psi_L(x,0)|^2 = {}^1/_2|\Psi_+ + \Psi_-|^2$, but at a time

$$\tau = \frac{\pi\hbar}{\Delta E} \tag{22}$$

the density $|\Psi_L(x,\tau)|^2 = {}^1/_2|\Psi_+ - \Psi_-|^2$; i.e., it has a maximum in the well on the right. We may then consider $\tau$ as the tunneling time.

In the case of an isolated triple well, we can still obtain a simple formula for $\tau$. We consider a symmetric splitting of the ground energy into $E_+$, $E_0$, and $E_-$ as the barriers decrease. Without loss of generality, we may set $E_0 = 0$. The state localized in the left well is, except for a time-independent factor

$$\Psi_L = \Psi_+ e^{-iEt/\hbar} + a\Psi_0 + \Psi_- e^{iEt/\hbar} \tag{23}$$

where $a$ is the constant coefficient required to localize the electron in the left well at $t = 0$. If $t = \tau = \pi\hbar/2E$, then $|\Psi_L|^2$ shows a maximum in the central well. We may rewrite $\tau = \pi\hbar/\Delta E$, where $\Delta E$ is the abovementioned splitting. Again $\tau$ has the meaning of tunneling time.

If the number of wells increases simple formulas for $\tau$ cannot be obtained, but we can assume eq 22 to be (approximately) valid regardless of the number of wells. At the limit of infinite wells, $\Delta E$ represents the bandwidth. Therefore, this assumption goes along the same lines as the reciprocal relationship between tunneling time and bandwidth pointed out at the beginning of this section and shown in Table 1.

**TABLE 2: Tunneling Time $\tau$ (To Reach the Neighbor Cell) Calculated Using Eqs 16 and 17 (Corresponding to Simple Parabolic and Sinusoidal Band Models) and Also Using Eq 22**

| $\Delta\omega = \Delta E/\hbar$ (au) | $\pi/\Delta\omega$ (au) | $\tau_p$ (au) | $\tau_s$ (au) |
|---|---|---|---|
| 0.05 | 62.8 | 83 | 74 |
| 0.1 | 31.4 | 41.5 | 36.7 |
| 1 | 3.1 | 4.1 | 10.7 |
| 10 | 0.3 | 0.4 | 1.1 |

Since by increasing the number of wells results in a larger splitting,[15] we conclude that periodicity reduces tunneling time. It should be pointed out, however, that $\tau$ does not just depend on $\Delta E$. As we indicated previously in this section, the DOS also influences tunneling time. Thus, Table 2 collects tunneling times calculated with eq 22, $\tau = \pi\hbar/\Delta E = \pi/\Delta\omega$, and also from the time-dependent overlap coefficient for the two $E_p(k)$ and $E_s(k)$ energy dispersion models under consideration, eqs 14 and 15. As we can see in this table, the simple eq 22 may be useful to obtain an order of magnitude for $\tau$. To attain a greater insight into eq 22, we study the time evolution of several band models with the same bandwidth and different DOS dispersion models. The $E_s(k)$ model, eq 15, is also included for the sake of comparison.

The linear model, defined by

$$E_l(k) = \alpha\left|\frac{kb}{\pi}\right| \tag{24}$$

has a constant DOS. The quadratic model, eq 14, and the $n$th power energy dispersion model

$$E_n(k) = \alpha\left(\frac{kb}{\pi}\right)^n \tag{25}$$

have DOS proportional to $k^{-1}$ and $k^{-(n-1)}$, respectively.

Figure 3 plots, for the abovementioned models and an arbitrary bandwidth of 25 au, the time $\tau_G$ required by an electron to reach consecutive $G$ cells vs $G$. We have also included the estimation of $\tau_G$ given by the approximate eq 22. As can be seen, eq 22 and the linear model, eq 24, are almost indistinguishable. This extremely close behavior can be understood if we remember that eq 22 does not include DOS in the estimation of $\tau_G$ and that DOS is just a constant in the case of the linear model.

It can also be seen that in the series of models defined by eq 25, the slope of $\tau_G$ vs $G$ decreases as $n$ increases, with a limit of zero as $n \rightarrow \infty$. The near linearity of $\tau_G$ vs $G$ in the above models suggests a generalization of (approximate) eq 22:

$$\tau_G = \frac{a}{\Delta E/\hbar}G \tag{26}$$

where $a = \pi$ for a constant DOS, eq 22, and $a \approx 2$ for an ideal parabolic band (and almost the same value for the relatively similar model defined by eq 15).

### 6. Tunneling Time in Chains of Quantum Dots

In this section we consider a chain built of spherical homogeneous InAs quantum dots embedded in a GaAs matrix. Several dot sizes and interdot distances have been considered in order to obtain a set of different band gaps and widths. Tunneling along the ground and excited minibands have been calculated. Also chains built of antidots, i.e., two-shell GaAs/InAs nanocrystals with a GaAs barrier-acting core and an InAs external well-acting clad embedded in a GaAs matrix, are also considered. Studying both kinds of systems is of interest because while the electrons are tightly attached to the nanodot center in homogeneous nanocrystals, they are distributed in the external shell and, then, loosely attached to the core, in the antidot system. Therefore, we may expect different conduction behaviors in each of the two cases.

The isolated quantum dot energy spectrum and electron densities are obtained by means of the **k·p** method and envelope function approximation (EFA).[8] Since the energy gap between bulk valence and conduction bands in these semiconductors is large (wide gap semiconductors) the conduction band can be successfully described by the one-band model. Then, we carry out the calculations within this approach which only requires an empirical parameter (the effective mass) to completely define the Hamiltonian (effective mass approach, EMA[9]). This parameter is fitted from the bulk and used in the quantum dot calculations.[16]

The potential energy part of the **k·p** Hamiltonian is a steplike potential that weakly confines the band electrons in the nanocrystal. In the case of homogeneous nanocrystals, this potential $V(r)$ is just a well whose height is given by the dot-matrix band off-set (or the electroaffinity of the quantum dot building block material, in the case of isolated quantum dots in a vacuum). In quantum antidots, the well for the electron motion is found in the external clad (and again, the corresponding barrier heights are equal to the band off-sets of the matching materials). The effective masses and band offsets employed in this paper are taken from ref 10.

For the sake of simplicity, we consider most symmetric, spherical nanocrystals. Then, the Hamiltonian has spherical symmetry and commutes with the angular momentum operator, so that the eigenvectors are labeled as if they were atoms: $nL_{M_z}$, where $L$, $M_z$ are the angular quantum numbers (indeed, quantum dots are often referred to as artificial atoms[11]).

When nanocrystals are arranged in a dense one-dimensional array, they interact and a lowering of symmetry from spherical to axial is produced. In parallel, individual discrete nanodot energy levels develop minibands as the quantum dot superlattice is formed. Since one-dimensional arrays have axial symmetry, cylindrical coordinates $(\rho,z)$ are used to solve the Hamiltonian eigenvalue equation numerically. The finite-differences method on a rectangular two-dimensional $(\rho,z)$ grid defined from $[0,-z_{max}]$ up to $[\rho_{max},z_{max}]$ is employed in the numerical procedure. Periodic boundary conditions on the $z$-axis, namely $\phi(\rho,z+b) = e^{iqb}\phi(\rho,z)$, where $b$ is the super lattice constant and $0 < q < \pi/b$, are employed for this coordinate. The boundary conditions that we impose in the directions perpendicular to the $z$-axis (i.e., on the $\rho$ coordinate) are the standard for bounded states of nonperiodic systems, namely, $\phi(\rho_{max},z) = 0$ (this condition being replaced by $(\partial\phi/\partial\rho)_{(0,z)} = 0$ for $M_z = 0$ states).

The above discretization of the differential equation that defines our model yields eigenvalue problems of asymmetric, complex, huge, and sparse matrices that have been finally solved by means of the iterative Arnoldi factorization method[12] implemented in the ARPAC package.[13]

Once the energy dispersions are obtained following the abovementioned procedure, the tunneling time required by an electron, located in a given quantum dot in the chain (and therefore described by the corresponding nonstationary Wannier function) to go into another dot in the chain is calculated with eq 13.

Table 3 summarizes the $\tau_5$ values calculated for three different chains of nanocrystals, namely: chains built of homogeneous

**TABLE 3: Tunneling Time $\tau_5$ Calculated for Different Nanocrystal Chains**[a]

| | | $d = 0.0$ nm | | $d = 1.5$ nm | | $d = 3.0$ nm | |
|---|---|---|---|---|---|---|---|
| | | $\Delta E$ (meV) | $\tau_5$ (au) | $\Delta E$ (meV) | $\tau_5$ (au) | $\Delta E$ (meV) | $\tau_5$ (au) |
| | $B_1$ | 17.39 | 20 024 | 5.36 | 65 097 | 1.74 | 20 0738 |
| HL | $B_2$ | 84.36 | 4194 | 30.07 | 11 620 | 11.01 | 31 710 |
| | $B_3$ | 136.78 | 2556 | 61.05 | 5694 | 26.60 | 13 112 |
| | $B_1$ | 34.63 | 10 035 | 11.23 | 31 079 | 3.78 | 92 450 |
| HS | $B_2$ | 155.83 | 2298 | 61.52 | 5690 | 24.73 | 14 122 |
| | $B_3$ | 186.81 | 1777 | **101.22** | **3343** | 54.39 | 6351 |
| | $B_1$ | 6.15 | 56 695 | 21.15 | 16 090 | 15.47 | 22 158 |
| A | $B_2$ | 32.69 | 10 745 | 68.67 | 5908 | 41.48 | 8997 |
| | $B_3$ | 59.97 | 6051 | **103.82** | **4010** | 56.84 | 6475 |

[a] Namely, a chain built of 8 nm radius homogeneous InAs QDs (HL), a chain built of 6.5 nm radius homogeneous InAs QDs (HS), and chains built of two-shell GaAs/InAs antidots, 8 nm core and 2 nm shell (A), for three interdot distances ($d = 0$ represents touching dots) and three lowest $M_z = 0$ minibands (B1 being the ground miniband).

InAs QDs with a radius of 8 nm (HL), chains built of homogeneous InAs QDs with a radius of 6.5 nm (HS), and chains built of GaAs/InAs antidots with an 8 nm radius GaAs core capped by a 2 nm InAs shell (A). Three interdot distances, $d = 0$ (touching dots), $d = 1.5$ nm, and $d = 3$ nm, and three lowest B1, B2, and B3 $M_z = 0$ minibands have been considered. For the sake of completeness, bandwidths are also enclosed in Table 3.

We can see from Table 3 that the chain built of small homogeneous nanocrystals (HS) shows lower $\tau_5$ values (and thus, higher electron mobilities) than the chain built of large homogeneous nanocrystals (HL). We can also see that for chains built of homogeneous QDs, the higher the nanocrystal density is, the lower the $\tau_5$ tunneling times and the higher the electron mobilities will be. This is not the case of the chain built of antidots (A) whose electron mobility rises as the QDs get closer, reaches a maximum for a given value of interdot distance $d$ (which is quite similar but not exactly the same for the different minibands under study) and finally decreases as they get closer until they touch each other. This behavior is related to the fact that the minibands cross for a given density and the structure reveals a semimetallic character. However, when the nanocrystals overlap by more than a given threshold, the minibands start to overlap, and then, new minigaps open at the crossing points and the structure loses the attained semimetallic character.

In general, the electron mobility in the ground 1B miniband is smaller than in the excited 2B, 3B minibands, the bandwitdth becomes narrower, and the calculated miniband dispersion is nearly parabolic with zero derivatives at the band edges (so that almost all calculated $\tau_5$ values may be approximated by eq 26 with $a \approx 2.14$). However, DOS also plays a role. We can see in Table 3 that the 3B bandwidth of a chain having an interdot distance $d = 1.5$ nm and built of small QDs (HS) is similar to the one with the same characteristics but built of antidots (A) (10.122 and 10.383 eV, respectively). Hence, one may expect that the antidot-chain tunneling time $\tau_5$(A) will be just a little smaller than $\tau_5$(HS), since the antidot bandwidth is a bit wider. However, we can see from Table 3 that $\tau_5$(A) = 4010 au is quite a lot larger than $\tau_5$(HS) = 3343 au. By looking at the energy dispersion of the bands involved we can understand this flipping as coming from a different DOS in each of the two cases: while HS-dispersion is almost parabolic ($\tau_5$(HS) fits eq 26 if $a \approx 2.03$), A-dispersion is nearly linear ($\tau_5$(A) fits eq 26 if $a \approx 2.93$, which is a value close to $\pi$, corresponding to an ideal linear dispersion).

## 7. Concluding Remarks

In this paper, we have introduced the concept of time-dependent overlap between Wannier functions. It allows the tunneling time along 1D quantum dot superlattices to be calculated quickly and easy. A comparison of the electron mobility in 1D arrays of homogeneous and two-shell antidot nanocrystals has been also carried out. It is found that while a monotonic increase in electron mobility vs nanocrystal density takes place in chains of homogeneous nanocrystals, quite different behavior occurs in chains of antidots. First it grows as the QDs get closer, reaches a maximum for a given value of interdot distance $d$, and then decreases as the QDs get closer until they touch each other.

The proposed time-dependent overlap coefficient and the results obtained can be useful in the study and design of new electronic devices.

**Acknowledgment.** Financial support from UJI-Bancaixa P1-B2002-01 is gratefully acknowledged. The Spanish MECD FPU grant (J.L.M.) is also acknowledged.

## References and Notes

(1) (a) Flebbe, O.; Eisele, H.; Kalka, T.; Heinrichsdorff, F.; Krost, A.; Bimberg, D.; Dähne-Prietsch, M. *J. Vac. Sci. Technol. B* **1999**, *17*, 1639. (b) Heitz, R.; Kalburge, A.; Xie, Q.; Grundmann, M.; Chen, P.; Holffmann, A.; Madhukar, A. *Phys. Rev. B* **1998**, *57*, 9050. (c) Lee, S. C.; Dawson, R. L.; Malloy, K. J.; Brueck, S. R. J. *Appl. Phys. Lett.* **2001**, *79*, 2630.

(2) (a) Dıaz, J. G.; Jaskólski, W.; Planelles, J.; Aizpurua, J.; Bryant, G. W. *J. Chem. Phys.* **2003**, *119*, 7484. (b) Dıaz, J. G.; Planelles, J. *J. Phys. Chem. B* **2004**, *108*, 2873.

(3) Kouwenhoven, L. P.; Hekking, F. W. J.; van Wees, B. J.; Harmans, C. J. P. M.; Timmering C. E.; Foxon, C. T. *Phys. Rev. Lett.* **1990**, *65*, 361.

(4) Brum, J. A. *Phys. Rev. B* **1991**, *43*, 12082.

(5) Wacker, A. *Phys. Rep.* **2002**, *357*, 1.

(6) Kohn, W. *Phys. Rev.* **1959**, *115*, 809.

(7) Marzari, N.; Vanderbilt, D. *Phys. Rev. B* **1997**, *56*, 12847.

(8) (a) Sercel, P. C.; Vahala, K. J. *Phys. Rev. B* **1990**, *42*, 3690. (b) Efros, Al. L.; Rosen, M. *Phys. Rev. B* **1998**, *58*, 7120.

(9) Bastard, G. *Wave Mechanics Applied to Semiconductor Heteroestructures*; Les Éditions de Physique: Les Ulis, France, 1988.

(10) Cao, Y. W.; Banin, U. *Am. J. Chem. Soc.* **2000**, *122*, 9692.

(11) Cheng, S. J.; Sheng, W. D.; Hawrylak, P. *Phys. Rev. B* **2003**, *68*, 235330.

(12) (a) Arnoldi, W. E. *Q. J. Appl. Math.* **1951**, *9*, 17. (b) Saad, Y. *Numerical Methods for large Scale Eigenvalue Problems*; Halsted Press: New York, 1992. (c) Morgan, R. B. *Math. Comput.* **1996**, *65*, 1213.

(13) (a) Lehoucq, R. B.; Sorensen, D. C.; Vu, P. A.; Yang, C. *ARPACK: Fortran subroutines for solving large scale eigenvalue problems, Release 2.1*; SIAM: Philadelphia, PA, 1998. (b) Lehoucq, R. B.; Sorensen, D. C.; Yang, C. *ARPACK User's Guide: Solution of Large-Scale Eigenvalue Problems with Implicit Restarted Arnoldi Methods*; SIAM: Philadelphia, PA, 1998.

(14) We write sin ($kb$/2) instead of the more common cos $kb$ because our cell is defined in [$-b$/2,$b$/2] instead of [0,$b$].

(15) It goes from $\Delta E = 2\beta$ in ethylene up to $\Delta E = 4\beta$ in polyacetylene, $\beta$ being the empirical resonance integral.

(16) In the present calculations, we have not included nonparabolicity effects on the effective mass.